Characteristic nanoscale deformation on a large-area coherent graphite moiré pattern

N. Sarkar, P. R. Bandaru, and R. C. Dynes

Phys. Rev. B **107**, L161402 — Published 5 April 2023

DOI: 10.1103/PhysRevB.107.L161402

Characteristic nanoscale deformation on a large-area coherent graphite moiré pattern

N. Sarkar[1*], P.R. Bandaru,[1,3] R.C. Dynes[2,3*]

[1]Department of Mechanical Engineering, [2]Department of Physics,

[3]Program in Materials Science,

University of California San Diego, La Jolla, California 92093-0411, USA

Highly oriented pyrolytic graphite (HoPG) may be the only known monatomic crystal with the ability to host naturally formed moiré patterns on its cleaved surfaces, which are coherent over micrometer scales and with discrete sets of twist angles of fixed periodicity. Such an aspect is in marked contrast to twisted bilayer graphene (TBG) and other multilayered systems, where the long-range coherence of the moiré is not easily maintained due to twist angle disorder. We investigate the electronic and mechanical response of coherent graphite moiré patterns through inducing external strain from STM tip-induced deformation. Consequently, unique anisotropic mechanical characteristics are revealed. For example, a lateral widening of one-dimensional (1D) domain walls (DWs) bridging Bernal (ABA) and rhombohedral (ABC) stacking domains (A, B and C refer to the atomic layer positioning), was indicated. Further, *in situ* tunneling spectroscopy as a function of the deformation indicated a tendency towards increased electrical conductance, which may be associated with a higher density of electronic states, and the consequent *flattening* of the electronic energy band dispersion. Such features were probed across the DWs, with implications for strain-induced electronic modulation of the moiré characteristics.

The natural occurrence of periodic and coherent moiré patterns unaffected by defects on exfoliated HoPG surfaces over large areas may be associated with the energetically favorable nature of superlattice formation (1). Consequently, HoPG may be considered a reliable experimental platform for investigating the effects of intrinsic and extrinsic strain (2) and the related modulation of electronic energy dispersion(3). Such “soft”(4) graphite surfaces could be probed by STM topography and spectroscopy and reveal electromechanical characteristics beyond those observed on twisted bilayer graphene (TBG) and other 2D-like materials systems. While TBG moiré modulated through hetero-strain(5,6), electrical gating(7), tip-induced deformation(8) or hydrostatic pressure(9) are interesting for the possibilities of superconductivity(10) and electronic flat bands(11), it is well known(12) that such systems are yet prone to surface defect induced-incoherent moiré. Alternatively, the moiré on atomically flat HoPG would be less influenced by such surface defects and can also be an ideal substrate for fabricating large scale coherent moiré patterns. The wider possibility of domain arrangements in graphite moiré, *i.e.,* AA, ABA, ABC, also yields a richer variety of topological configurations that may be investigated.

Atomic sheets constituting the HoPG are coupled by weak van der Waals (vdW) forces that allow cleavage of the constituent layers along the basal planes. Often, the partially lifted layers in cleavage reattach to the HoPG surface, with rotation, to form a moiré pattern as shown in **Fig. 1(a)**. We have observed the occurrence of multiple discrete sets of moiré patterns of varying twist angles (θ_{twist}) with corresponding periodicities. In contrast, in TBG synthesized through chemical vapor deposition(13) or dry transfer(12), incoherent periodicity in the moiré is nominally observed *i.e.,* a twist angle disorder, presumably due to the inevitable occurrence of defects(12) related to substrate roughness, polymer residues, wrinkles, *etc*. However, moiré on HoPG is less susceptible to such disorder, and defects such as wrinkles or steps may instead act as pinning centers yielding discrete changes in θ_{twist}**: Fig. 1(a)** - *also see Figure S1 in Supplementary section S1*(14)). The tilt boundaries marking the edges of the moiré superlattices are denoted by arrays of orange dots in **Fig**. **1(a)** and seem displaced out of the plane indicating highly strained regions or *tilt boundaries* (*see Supplementary section S1*(14)).

An instance of a graphite moiré pattern with θ_{twist} = 4.2° is shown in **Figs. 1(b)** and **1(c).** The periodic occurrence of the AA domains (hill-like features), ABA domains (valley-like features) and the bridging DWs is illustrated. The AA atom stacking is an unstable configuration due to direct placement of atoms on the individual layers on top of each other while the ABA/Bernal stacking is more stable with an atom from the top layer occupying the spaces between the atoms of the lower layer or *vice versa*. In this work, STM tip-induced surface deformation(4,15) of moiré patterns was used for revealing local vdW bonding strength variability(1,16) across the moiré landscape as well as elastic mechanical deformation characteristics perpendicular to the surface, as indicated through the schematic of **Fig. 2(a).** The STM tip was scanned in the direction: AA → DW → AA: *blue dashed line*, or along AA→ABA→ AA: *black dashed line*, as indicated in **Fig. 1(c).** The related topography is shown as a function of the tunneling current (I_{tip}) in **Fig. 2(b)** and *Supplementary section S2*(14).

The observed high (/low) surface deformation amplitude in the AA (/ABA) domains could be ascribed to the associated weaker (/stronger) vdW bonding while the bonding in the DW region itself appears intermediate to that relative to the AA (/ABA) stacking. The deformation amplitudes of the domains measured from **Figs. 2(b)** and **S2(b)** are indicated in **Fig. 2(c) -** as a function of the I_{tip} and R_{gap} (tunneling gap resistance = V_{sample}/I_{tip}, with V_{sample} as the applied bias voltage on the HoPG). At a reduced tip-sample gap, *i.e.,* with lower R_{gap}, there is considerable outward deformation*/bulging* out of the unstable AA stacking by ~ 1.1 nm whereas the ABA regions are

much less deformed, *i.e.,* at ~ 0.3 nm, due to stable stacking configurations and stronger bonding. The high amplitude of these deformations dominate over the electronic states variation in topography maps. Hence, a topographic map of the graphite moiré could be considered a map of its relative interlayer vdW strength. Tip-induced deformations on "soft" HoPG(4) would be of much higher magnitude relative to TBG(8,15) due to the larger influence from the substrate in the latter case. To guard the tip shape and geometry during deformation, small tunneling resistances (~kΩ) corresponding to small gap distances were avoided. In addition to the surface deformations of domains, tip-induced atomic forces also pull individual atoms. The *inset* in **Fig. 2(b)** indicates enhanced atomic corrugations on AA domains compared to those on ABA sites and are plotted in **Fig. 2(d)**. It was observed here that the AA domains appear less rigid relative to the ABA domains.

Any external strain induced by the STM tip would be expected to deform the moiré surface features anisotropically, with deformation perpendicular to the surface, expected to be larger than in the surface plane(1,8,11). We show such asymmetry in the mechanical characteristics through monitoring STM tip-induced deformation as a function of θ_{twist}. The moiré patterns with θ_{twist} of 4.2^o and 0.5^o are shown before deformation in **Figs. 3(a**) and **3(b)** and after deformation (through an increased I_{tip}) in **Fig. 3(c)** and **Fig. 3(d),** respectively. The transition of the original moiré pattern to a deformed one with tip-induced deformation was reversible over the chosen range of operation. For θ_{twist} = 4.2^o, the AA regions ("hills") relatively occupy the same surface area in topography maps as the ABA regions ("valleys") before and after the deformation: **Fig. 3(a)** and **Fig. 3(b)**. The relative surface area occupied by the moiré domains is a measure(17) of the local strain energy balance. However, with θ_{twist} reduction from 4.2^o to 0.5^o: **Fig. 3(a)** and **Fig. 3(c)**, it was observed that (i) the periodicity of the AA domains has increased by an order of magnitude from ~ 3 nm to ~ 30 nm, (ii) triangular patterns of ABC and ABA domains become dominant, and there is a (iii) pronounced stretching of DWs into linear structures. Domain Walls occupy narrow spaces between ABA and ABC stacked domains with a gradient in stacking configuration(13) and are thus relatively less stable stacking regions. Consequent to deformation in **3(d)**, the 1D DWs stretch laterally into a 2D area shrinking the triangular ABC and ABA domains. Such longitudinal and lateral stretching behavior of DWs may be related to their soliton-like nature(13). Indeed, DWs have previously been shown(18) to be elastic string-like and may be correspondingly deformed with the STM tip depending on the direction of approach towards the ABC(/ABA) boundary. Such behavior is obscured(8) in TBG systems due to the lack of rhombohedral ABC domains.

To further probe the deformation characteristics along the direction perpendicular to the surface, the topography in the undeformed and deformed moiré patterns is compared in **Fig. 3(e)**. It was observed that prior to deformation (*black trace*), the ABC domains have a higher plateau compared to the ABA region indicating that ABA has stronger interlayer coupling than ABC. However, subsequent to deformation (*blue trace*), the AA domains are most affected out of plane, more than the ABC and the ABA domains. The ABA (*red label*) and ABC (*yellow label*) domains shrink in surface area while the DW (*green label*) region enlarges. The average deformation amplitude across the moiré surface, as a function of θ_{twist}, is indicated in **Fig. 3(f)** where the error bars correspond to atomic corrugations (*See Supplementary S2*(14)*)***.** A lower out-of-plane surface deformation is observed for small θ_{twist} : **Fig. 3(f).** However, in-plane, an opposite trend is observed in **Fig. 3(a)** to **(d)**, i.e. there is lateral deformation of domains for lower θ_{twist} = 0.5° with no change in higher θ_{twist} = 4.2°. Such anisotropic response, *i.e.,* of increased flexibility perpendicular to the surface and diminished flexibility coplanar with surface is observed when θ_{twist} is < 1° (*See Supplementary S3*(14)). The amplification of the moiré periodicity at the lower θ_{twist} (< 1°) allows stretching/straining of the DWs with an enlarged metastable ABC domain(1) which imparts an increased flexibility to the moiré domains in-plane only.

The gradual evolution of the lateral stretching of DWs with increased mechanical deformation, *i.e.,* increased I_{tip} increment (at a fixed V_{sample}) is shown in Fig. S4(a)→(c) *(See Supplementary Section S4*(14)*)*. The independence on V_{sample} (at fixed I_{tip}) implies minimal electronic influences(18) on the deformed pattern *(See Supplementary Section S4*(14)*)*. This deformation mechanism is consistent for several observed θ_{twist} < 1° *(See Supplementary Section S3*(14)*)* indicating purely mechanical deformation effects. Further, the deformation pattern was independent of the tip-scanning direction. The schematic of the undeformed and deformed moiré is mapped in **Fig. 3(g)**. The three-fold rotational symmetry(1) of the alternating ABC and ABA sites is maintained. The spatially pinned AA domain determines the intersections of all the DWs(13), which grow wider subsequent to deformation. From the 3D map in **Fig. 3(h)**, a gradient in topography is observed along the DWs as indicated by the arrows - from bright to dark- in **Fig. 3(g)** and may be ascribed to constituent electric polarizability(19). Indeed, the flexoelectric character(20) of DWs induced through strain gradients from STM tip-induced interactions could be indicated. These strain gradients are arranged similar(21) to the triangular networks of highly conductive 1D electronic channels(22) around AB/BA domains. Such a network have previously(23) exhibited Aharonov–Bohm oscillations whose periods correspond to one magnetic

flux quantum threading through the enclosed triangular domain areas only in TBG morphologies, and such effects may also be investigated in deformed graphite moiré.

The electronic DW channels merge at every metallic AA node where they can get coupled to further demonstrate weak Shubnikov-de Haas oscillations(22). Such AA sites have also been previously(19) attributed to a gapless *flat-band* energy dispersion associated with a high density of electronic states (DOS). Further enhancement of the DOS with tip-induced local strain induced is shown in **Fig. 4(a)** through an increased electrical conductance (*dI/dV*) probed on AA sites of θ_{twist} = 0.8°. The in-situ spectroscopy reveals the narrowing of the conductance peaks, with decreasing R_{gap}: **Fig. 4(a)** bottom to top. Such spectroscopy modulation is reproducible on repeated tip pulling in/out of the AA stacked layers. However, there is no observed difference in I(V) spectroscopy on AB-stacked HoPG surfaces before, during and after tip-induced deformation.

The conductance modulation through atomic tip-induced strain(11) can also be applied on distinctive electronic peaks of other domains and DWs. Such characteristic bias-specific peaks have previously(24) been shown on ABA/ABC domains but not on graphite DWs. In TBG, the DWs have been associated(22,24) with edge states which were predicted(25) to be difficult to probe in graphite moiré. The long-range coherence of graphite moiré favors conductance probing of electronic states gradually across the domains, *e.g.,* a typical path (*blue arrow*), AA → ABC → DW → ABA, is shown in **Fig. 4(b),** on a graphite moiré pattern of θ_{twist} ~ 1.1°. Here, unique bias-specific peaks were observed for the domains and domains walls: **Fig. 4(c)**. For instance, the peak at ~100 mV was associated with the AA domain from the high conductance and expected large DOS(19) with flat band characteristics. The single peak subsequently evolves into a pair when the ABC domains are probed - with a peak separation/gap (Δ_{ABC}) of ~ 50 mV. Such gap formation has been previously reported(24,26) along with its calculated band structure(24) shown in the top-left *inset* of **Fig. 4(c).** The Δ_{ABC} gradually disappears as the ABA domain is encountered. Here, a parabolic band energy dispersion was predicted(24) with the calculated band structure - shown in the top-right *inset* of **Fig. 4(c)**. While Δ_{ABC} could be increased through electrical gating(27,28) in TBG, this would not be possible on graphite moiré(25). Such an increased gap would be necessary for the existence of electrical field induced topological chiral edge modes at AB-BA domain walls(22,24). However, in graphite moiré, the edge modes related to the ABA-ABC DWs would be relatively dispersive(25) and difficult to probe. The set of peaks at ~300 mV (*green arrows*) in **Fig. 4(c)** observed close to the boundary between the ABC and ABA domains

could be associated with the corresponding DW. The peak at ~ 400 mV - seen on all the domains except ABA, suggests the possibility of a delocalized energy band(29).

The domain area modulations through atomic tip-induced strain would modify their electronic characteristics and suggest possibilities in the use of graphite moiré for highly sensitive and specific stress or pressure(9) sensors tunable at atomic scale. At a θ_{twist} = 1.1^o, the graphite Moiré is expected and was indeed observed to have different electronic spectroscopy signatures from that in TBG arising from the possibility of ABA/ABC domains in graphite moiré, in contrast to the AB/BA configuration in TBG. Also see *Supplementary Section S5*(14)*,* for the possibility of nematic phase formation(17,19) at such θ_{twist}. The deformation characteristics of domains and DWs, as elucidated in our work, is shown to be related to the weak interlayer interactions for multiple layered HoPG. However, the stronger physico-chemical influence of the substrates on 2D stacks like TBG possibly would make it difficult to observe such deformation phenomena.

In summary, STM based structural and spectroscopic investigations on graphite moiré yields new observations and insights, not evidenced in bilayer graphene moiré such as: (i) naturally occurring coherent graphite moiré over micron scale with discrete/discontinuous change in θ_{twist}, (ii) Crystallographic directions or θ_{twist} dependent mechanical deformation characteristics, (iii) lateral stretching of 1-D DWs into 2-D domains, mimicking soliton-like behavior, with strain gradients that may be related to electrical polarizability and indicating a topological transport network that may exhibit Aharonov-Bohm oscillations (iv) controlled relative surface area modulations of the moiré domains and DWs. The possibility of robust strain-induced modulation of electrical conductivity motivates the use of graphite moiré for sub-nanoscale displacement sensing devices.

Methods:

Materials

HoPG of low ZYH grade from Advanced Ceramics, Inc with micron sized grains favored the occurrence of surface defects like step heights or grain boundaries which would act as pinning sites for moiré pattern formation during cleavage.

Electrical Measurements

A custom-built scanning tunneling microscope (STM) with a RHK controller at room temperature and atmospheric pressure was used. The imaging was done at a nominal sample bias of 0.1V and tunneling current of 10nA. The topography measurements were performed in standard constant current mode at ~0.5 Hz scanning frequency using a mechanically snipped Pt/Ir tip. For surface deformation experiments, the tip was brought closer to the sample by varying the

tunneling currents from 10 nA to 100 nA. Tunneling spectroscopy measurements utilized a lock-in modulation of 3mV at 5kHz to the sample bias which was swept from -0.4V to 0.5V.

Calibration and Data analysis

The reported topographic length scales in-plane (x, y) and out-of-plane (z) were calibrated through atomic lattice constants of graphite through atomic imaging of the surface and its monatomic step. The surface deformation amplitudes were averaged over five moiré unit cells and the atomic corrugation estimation were averaged over ten atomic unit cells. The error bars estimation for surface deformation amplitude measurement in Fig. **3(e)** is described in Supplementary Section S2(14). All the imaging and deformation measurements were done using the same tip. All images were measured with V_{sample} is 100 mV. All domains are color coded: AA (*pink*), ABA (*red*), ABC (*yellow*) and DW (*green*).

References:

1. M. M. Van Wijk, A. Schuring, M. I. Katsnelson and A. Fasolino. Relaxation of moiré patterns for slightly misaligned identical lattices: Graphene on graphite. *2d Mater* **2**, 034010 (2015).
2. M. Szendro, A. Pálinkás, P. Süle and Z. Osváth. Anisotropic strain effects in small-twist-angle graphene on graphite *Phys Rev B* **100**, 125404 (2019).
3. R. Bistritzer and A. H. MacDonald. Moiré bands in twisted double-layer graphene. *Proceedings of the National Academy of Sciences* **108**, 12233 (2011).
4. J.M. Soler, A. M. Baro, N. Garcia and H. Rohrer. Interatomic forces in scanning tunneling microscopy: giant corrugations of the graphite surface. *Phys Rev Lett* **57**, 444 (1986).
5. L. Huder, A. Artaud, T. Le Quang, G. T. De Laissardiere, A. G. Jansen, G. Lapertot, C. Chapelier and V. T. Renard. Electronic Spectrum of Twisted Graphene Layers under Heterostrain. *Phys Rev Lett* **120**, 156405 (2018).
6. F. Miao, S. J. Liang and B. Cheng. Straintronics with van der Waals materials. *NPJ Quantum Mater* **6**, 59 (2021).
7. X. Liu, C. L. Chiu, J.Y. Lee, G. Farahi, K. Watanabe, T. Taniguchi, A. Vishwanath and A. Yazdani. Spectroscopy of a tunable moiré system with a correlated and topological flat band. *Nature Communications* **12**, 2732 (2021).
8. M. Yankowitz, K. Watanabe, T. Taniguchi, P. San-Jose and B. J. Leroy. Pressure-induced commensurate stacking of graphene on boron nitride. *Nat Commun* **7**, 13168 (2016).
9. Z. Wu, X. Kuang, Z. Zhan and S. Yuan. Magic angle and plasmon mode engineering in twisted trilayer graphene with pressure. *Phys Rev B* **104**, 205104 (2021).
10. M. Yankowitz, S. Chen, H. Polshyn, Y. Zhang, K. Watanabe, T. Taniguchi, D. Graf, A. F. Young and C. R. Dean. Tuning superconductivity in twisted bilayer graphene. *Science* **363**, 1059 (2019).
11. F. Mesple, A. Missaoui, T. Cea, L. Huder, F. Guinea, G. T. de Laissardiere, C. Chapelier, and V. T. Renard. Heterostrain Determines Flat Bands in Magic-Angle Twisted Graphene Layers. *Phys Rev Lett* **127**, 126405 (2021).

12. A. Uri, S. Grover, Y. Cao, J. A. Crosse, K. Bagani, D. Rodan-Legrain, Y. Myasoedov, K. Watanabe, T. Taniguchi, P. Moon and M. Koshino. Mapping the twist-angle disorder and Landau levels in magic-angle graphene. *Nature* **581**, 47 (2020).
13. J.S. Alden, A. W. Tsen, P. Y. Huang, R. Hovden, L. Brown, J. Park, D.A. Muller and P. L. McEuen. Strain solitons and topological defects in bilayer graphene. *Proceedings of the National Academy of Sciences* **110**, 11256 (2013).
14. See Supplemental Material at [URL] for (i) details on role of surface defects in forming moiré patterns, (ii) surface deformation estimates from topographic line scans, (iii) twist angle dependence with deformed moiré patterns, (iv) minimal electronic influences on deformed moiré patterns, (v) for possible nematic phase formation at 1.1^{o} twist angle.
15. N. Sarkar, P. R. Bandaru and R. C. Dynes. Probing interlayer van der Waals strengths of two-dimensional surfaces and defects, through STM tip-induced elastic deformations. *Nanotechnology* **35**, 15LT01 (2023).
16. E. N. Voloshina, Y. S. Dedkov, S. Torbrügge, A. Thissen, M. Fonin. Graphene on Rh(111): Scanning tunneling and atomic force microscopies studies. *Appl Phys Lett* **100**, 241606 (2012).
17. N. P. Kazmierczak, M. Van Winkle, C. Ophus, K. C. Bustillo, S. Carr, H. G. Brown, J. Ciston, T. Taniguchi, K. Watanabe and D. K. Bediako. Strain fields in twisted bilayer graphene. *Nat Mater* **20**, 956 (2021).
18. M. Yankowitz, J. I. J. Wang, A. G. Birdwell, Y. A. Chen, K. Watanabe, T. Taniguchi T, P. Jacquod, P. San-Jose, P. Jarillo-Herrero and B. J. LeRoy. Electric field control of soliton motion and stacking in trilayer graphene. *Nat Mater* **13**, 786 (2014).
19. A. Kerelsky, L. J. McGilly, D. M. Kennes, L. Xian, M. Yankowitz, S. Chen, K. Watanabe, T. Taniguchi, J. Hone, C. Dean and A. Rubio. Maximized electron interactions at the magic angle in twisted bilayer graphene. *Nature* **572**, 95 (2019)
20. L. J. McGilly, A. Kerelsky, N. R. Finney, K. Shapovalov, E. M. Shih, A. Ghiotto, Y. Zeng, S. L. Moore, W. Wu, Y. Bai and K. Watanabe. Visualization of moiré superlattices. *Nat Nanotechnol* **15**, 580 (2020).
21. C. De Beule, F. Dominguez and P. Recher. Aharonov-Bohm Oscillations in Minimally Twisted Bilayer Graphene. *Phys Rev Lett* **125**, 096402 (2020).
22. L. Ju, Z. Shi, N. Nair, Y. Lv, C. Jin, J. Velasco Jr, C. Ojeda-Aristizabal, H. A. Bechtel, M. C. Martin, A. Zettl and J. Analytis. Topological valley transport at bilayer graphene domain walls. *Nature* **520**, 650 (2015).
23. S. G. Xu, A. l. Berdyugin, P. Kumaravadivel, F. Guinea, R. Krishna Kumar, D. A. Bandurin, S. V. Morozov, W. Kuang, B. Tsim, S. Liu and J. H. Edgar. Giant oscillations in a triangular network of one-dimensional states in marginally twisted graphene. *Nat Commun* **10**, 4008 (2019).
24. L. J. Yin, H. Jiang, J. Bin Qiao and L. He. Direct imaging of topological edge states at a bilayer graphene domain wall. *Nat Commun* **7**, 11760 (2016).
25. K. Zou, F. Zhang, C. Clapp, A. H. MacDonald and J. Zhu. Transport studies of dual-gated ABC and ABA trilayer graphene: Band gap opening and band structure tuning in very large perpendicular electric fields. *Nano Lett* **13**, 369 (2013).
26. M. Koshino and E. McCann. Trigonal warping and Berry's phase Nπ in ABC-stacked multilayer graphene. *Phys Rev B Condens Matter Mater Phys* **80**, 165409 (2009).

27. J. Yan and M. S. Fuhrer. Charge transport in dual gated bilayer graphene with corbino geometry. *Nano Lett* **10**, 4521 (2010).
28. W. Yao, S. A. Yang and Q. Niu. Edge states in graphene: From gapped flat-band to gapless chiral modes. *Phys Rev Lett* **102**, 096801 (2009).
29. S. Hattendorf, A. Georgi, M. Liebmann and M. Morgenstern. Networks of ABA and ABC stacked graphene on mica observed by scanning tunneling microscopy. *Surf Sci* **610**, 53 (2013).

Acknowledgements:
This work was supported by AFOSR Grant (FA9550-15-1-0218) and Army Research Office (AROW911NF-21-1-0041). The authors wish to thank Michael Rezin for the technical assistance; Prof. Shane Cybart and Dr. Uday Sravan Goteti for useful discussions.

Author contributions:
N. Sarkar did the experimental work and along with P.R. Bandaru and R.C. Dynes, wrote the paper. All analysis and discussion were under the supervision of R.C. Dynes and P.R. Bandaru.

Data availability:
The experimental data and its analysis in the paper and/or in the supplementary information is sufficient to support our conclusions. Additional data can be made available on request.

Competing interests:
The authors declare no competing interests.

Figures

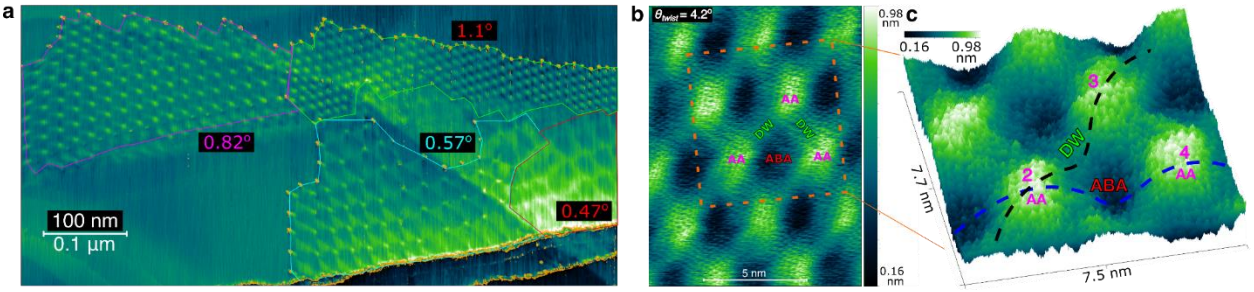

Figure 1: **Moiré patterns on graphite surface and related domain features. (a)** The occurrence of coherent moiré over micron scales with multiple twist angles (θ_{twist}) in degrees. **(b)** The observed domain pattern, at a θ_{twist}=4.2°, with the AA domains (*bright* hill-like features), ABA domains (*dark* valley-like features) and the bridging domain walls (DWs). **(c)** Atomically resolved three-dimensional topography of a region from **(b).** The small dots correspond to individual atoms.

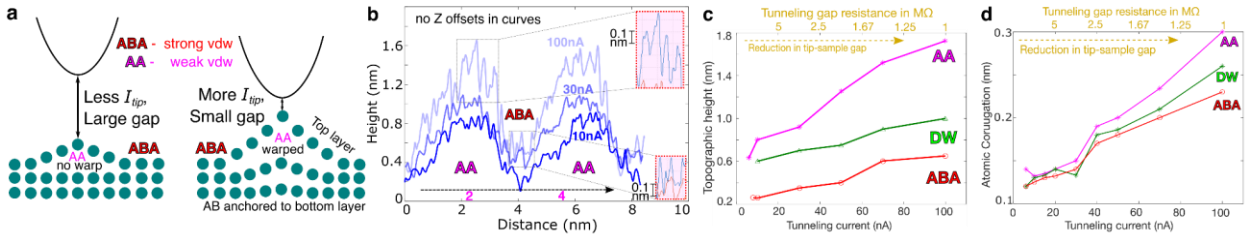

Figure 2: **STM tip induced deformation of moiré domains. (a)** Surface deformation by STM tip through large(/small) atomic forces monitored through large(/small) tunneling currents at smaller(/larger) tip-sample distance. **(b)** Topographic line scans along AA → ABA → AA: *black dashed line* in figure **1(c)** with no z-offset indicating out-of-plane surface deformation. A larger (/smaller) extent of surface deformation and atomic corrugation is seen in **(c)** and **(d)** for the AA (/ABA) domains with an intermediate extent for the DWs.

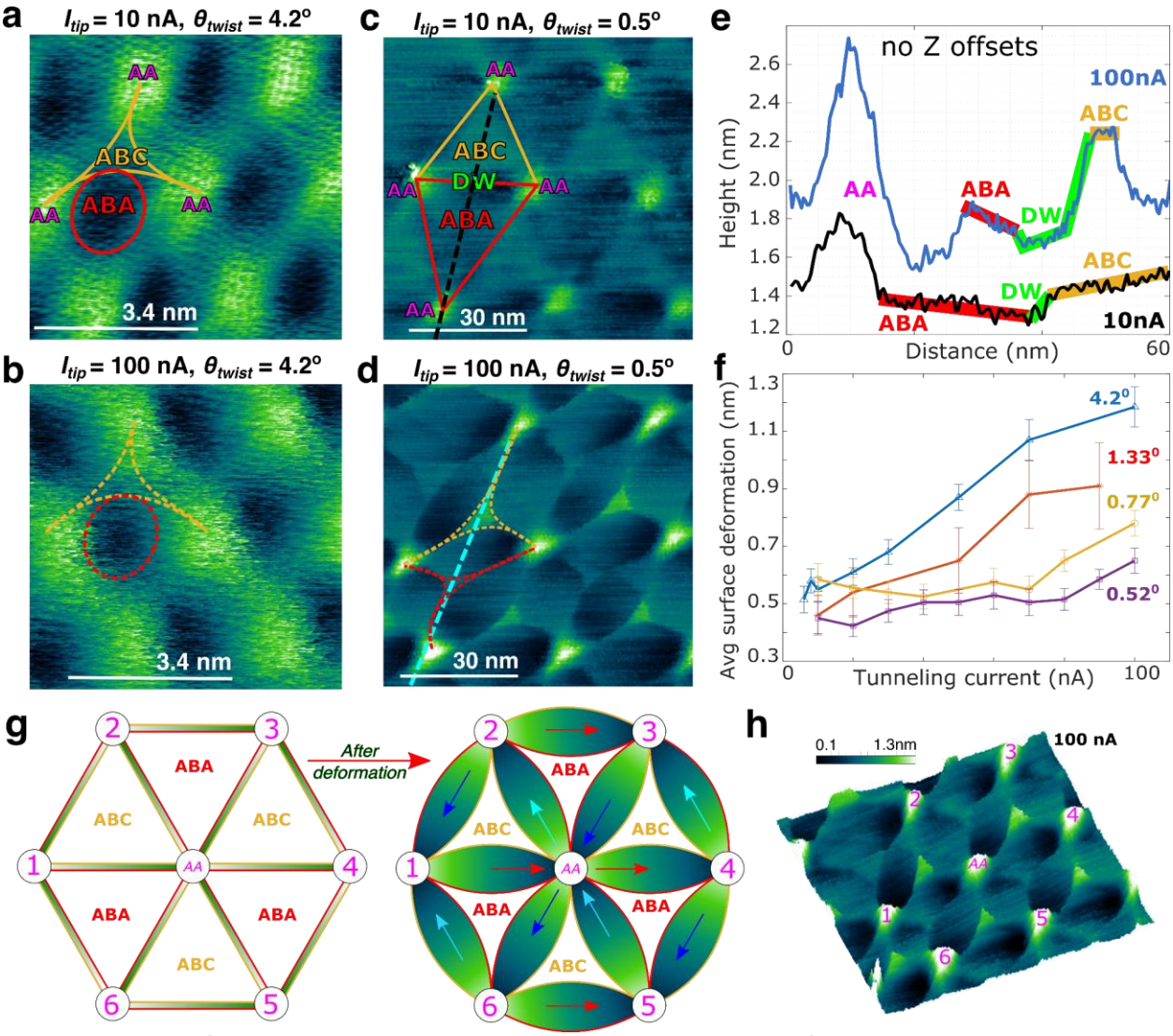

Figure 3: **Moiré twist angle dependent deformation.** Moiré patterns before and after deformation are shown for θ_{twist} = 4.2° in **(a)** and **(b)** as well as for θ_{twist} = 1.1° in **(c)** and **(d)** respectively. The AA domain periodicities and θ_{twist} remain unchanged. The ABA and ABC domains shrink after deformation for θ_{twist} = 1.1° but no change is observed for θ_{twist} = 4.2°. **(e)**

The topography traced along the *black* and *blue* dotted lines in **(c)** and **(d)** as a function of I_{tip} indicates an out of plane displacement for the domains in the order AA > ABC > ABA. **(f)** Larger average deformation is observed for lower θ_{twist} as a function of I_{tip}. **(g)** The domain pattern exhibits a three-fold symmetry, with AA as an origin (left), and this symmetry is unaltered by tip-induced deformation (right) as also evident from the 3D topographic image in **(f)**. ABA/ABC domains shrink while DWs grow wider and the gradient in topography along the DWs - indicated by the arrows from bright to dark with similar electronic DW network like in TBG exhibiting Aharonov-Bohm effects.

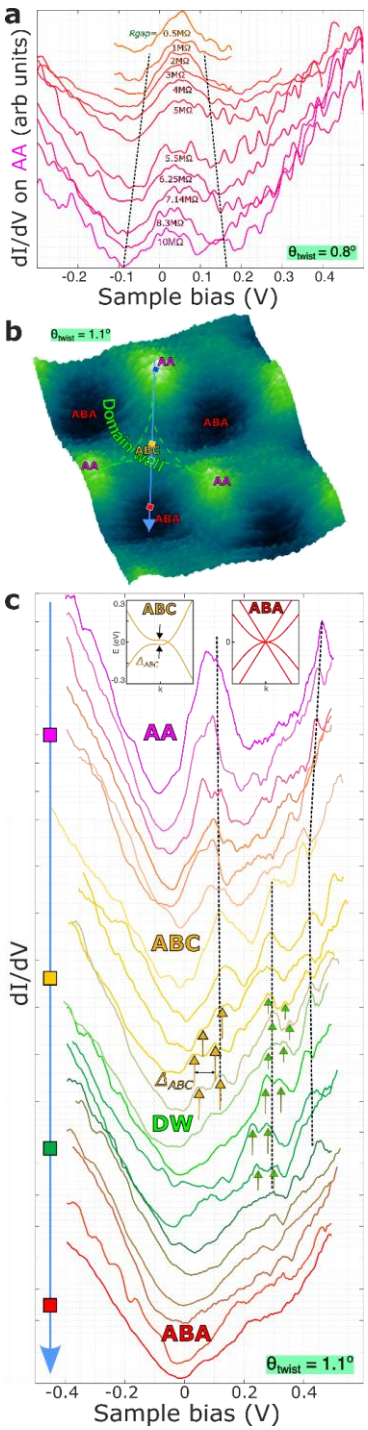

Figure 4: **Electrical conductance mapping across moiré domains. (a)** For a moiré with θ_{twist} = 0.8°, the zero-bias conductance peak on the AA domain narrows with a reduced R_{gap}. **(b)** Moving with the STM tip along the *blue* arrow, on a moiré with θ_{twist} = 1.1° across the domains: AA (*pink*) → ABC (*yellow*) → DW (*green*) → ABA (*red*), yields conductance traces as shown in **(c)** with distinctive spectroscopy at ~100 mV and ~300 mV and related band structure shown in the top-left and top-right *inset*.